Supporting Information

Scalable Ultrarobust Thermoconductive Nonflammable Bioinspired Papers of Graphene Nanoplatelets Crosslinked Aramid Nanofibers for Thermal Management and Electromagnetic Shielding

Minh Canh Vu[a], Pyeong Jun Park[b], Sa-Rang Bae[c], Soo Young Kim[c], Young-Min Kang[d], Won Kook Choi[e], Md Akhtarul Islam[f], Jong Chan Won[g], Manbok Park[i], Sung-Ryong Kim[a,*]

[a]*Department of Polymer Science and Engineering, Korea National University, Chungju 27469, Republic of Korea.*

[b]*School of Liberal Arts and Sciences, Korea National University of Transportation, Chungju 27469, Republic of Korea.*

[c]*Department of Material Science and Engineering, Korea University, Seoul 02841, Republic of Korea.*

[d]*Department of Material Science and Engineering, Korea National University of Transportation, Chungju 27469, Republic of Korea.*

[e]*Center for Optoelectronic Materials and Devices, Korea Institute of Science and Technology, Seoul 02792, Republic of Korea.*

[f]*Department of Chemical Engineering and Polymer Science, Shahjalal University of Science and Technology, Sylhet-3114, Bangladesh.*

[g]*Advanced Materials Division, Korea Research Institute of Chemical Technology, Daejeon, 34114, Republic of Korea.*

[i]*Department of Electronic Engineering, Korea National University of Transportation, Chungju 27469, Republic of Korea.*

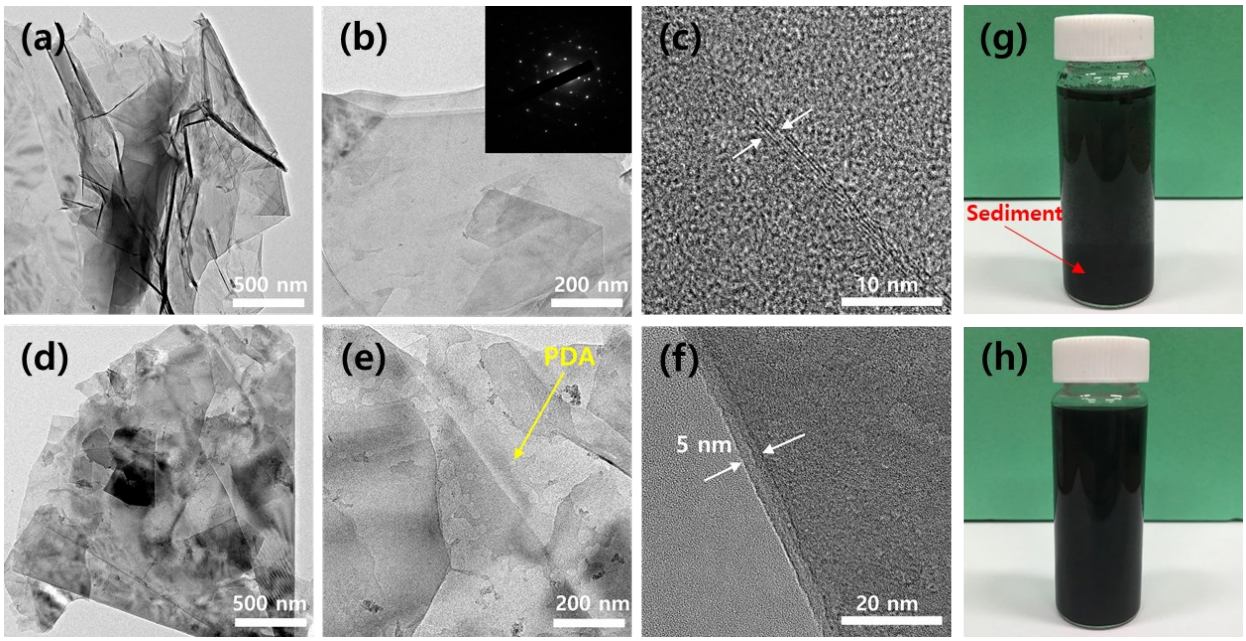

Figure S1. TEM images of (a-c) purified GnP and (d-f) fGnP filler. Digital photos of (g) purified GnP and (h) fGnP in DI water.

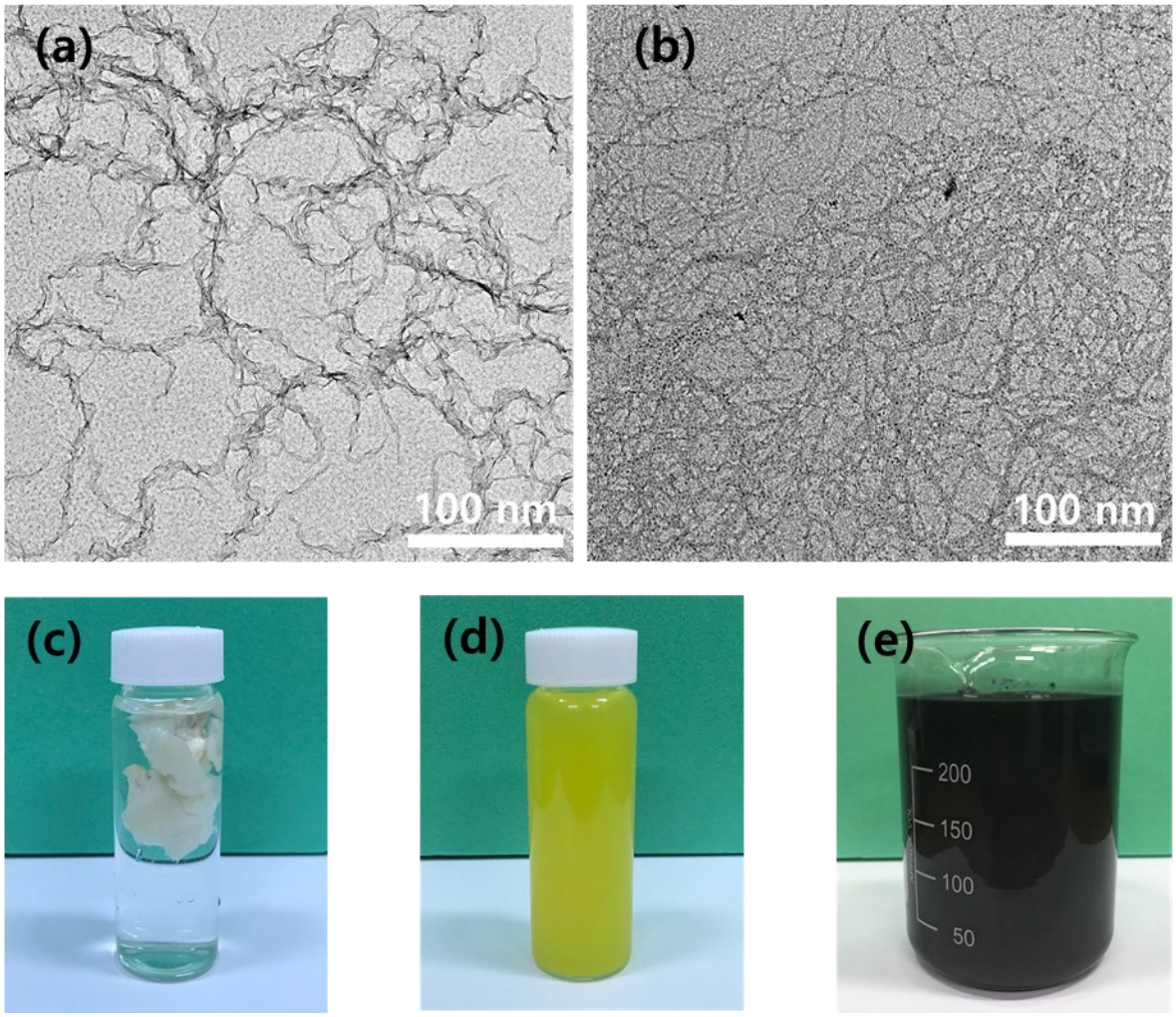

Figure S2. TEM images of (a) pristine ANF and (b) acid treated ANF. Digital photos of (c) ANF in DI water, (d) oANF in DI water and (e) The mixture of fGNP and oANF suspension after a month.

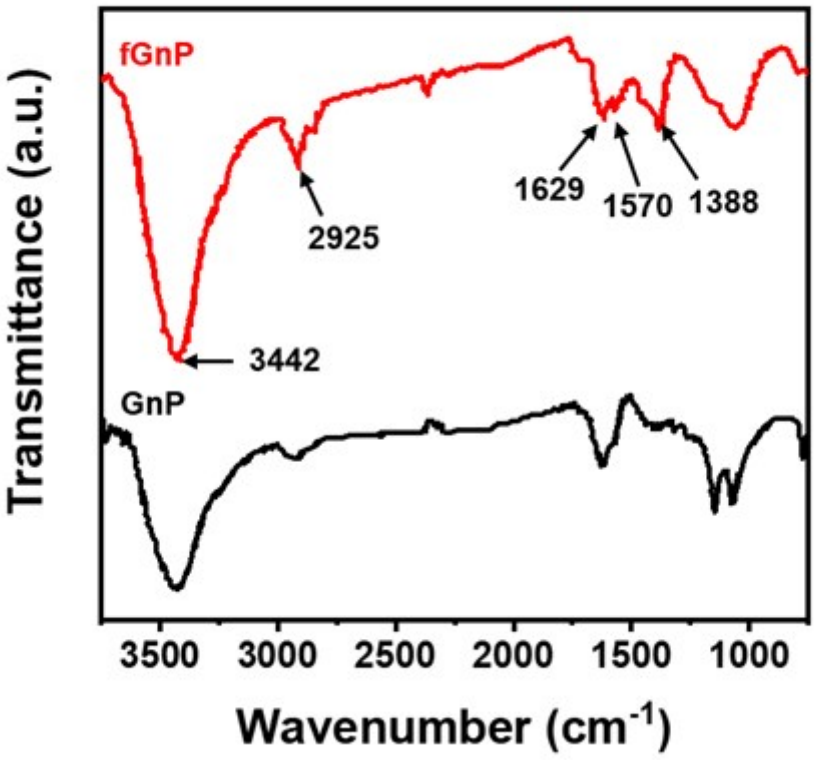

Figure S3. FTIR spectra of GnP and fGnP.

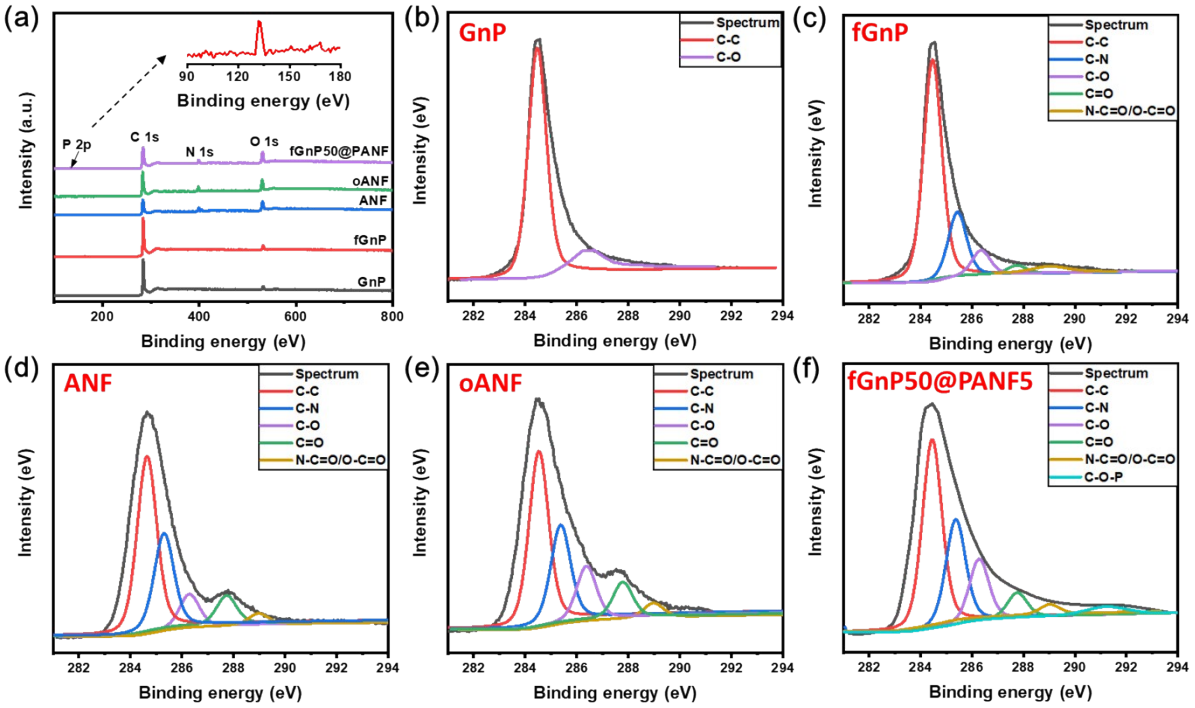

Figure S4. (a) Survey XPS spectra of GnP, fGnP, ANF, oANF and fGnP50@PANF5, (b-f) High-resolution of C 1s spectra of GnP, fGnP, ANF, oANF and fGnP50@PANF5.

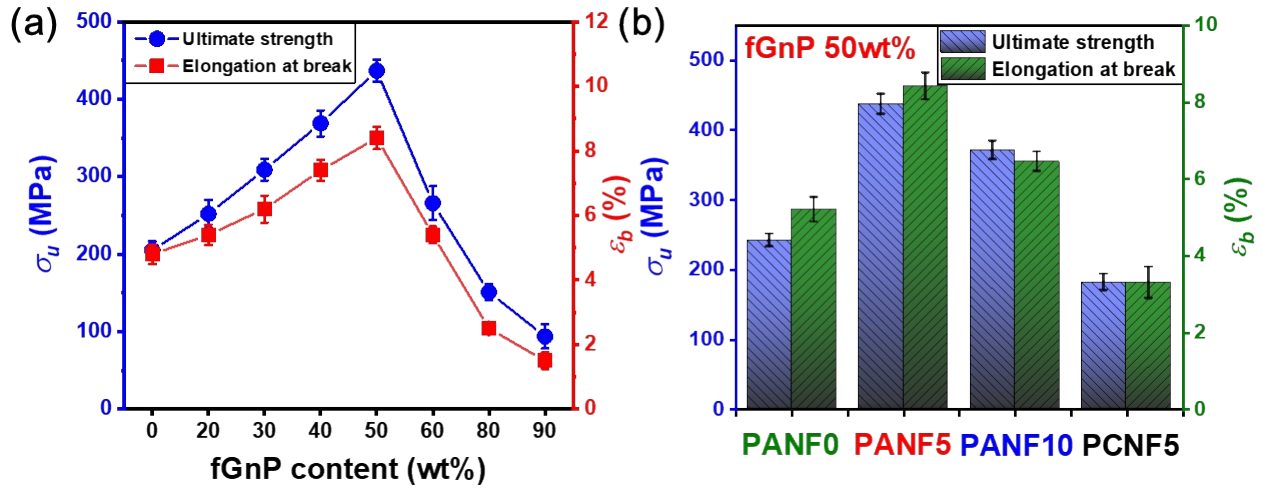

Figure S5. (a) Ultimate tensile strength (σ_u) and elongation at break (ε_b) of fGnP@PANF (crosslinked with 5 wt% of PNCT) as a function of fGnP content, (b) Ultimate tensile strength and elongation at break of fGnP50@PANF0 (0 wt% of PNCT), fGnP50@PANF5 (5 wt% of PNCT), fGnP50@PANF10 (10 wt% of PNCT), and fGnP50@PCNF5 (5 wt% of PNCT).

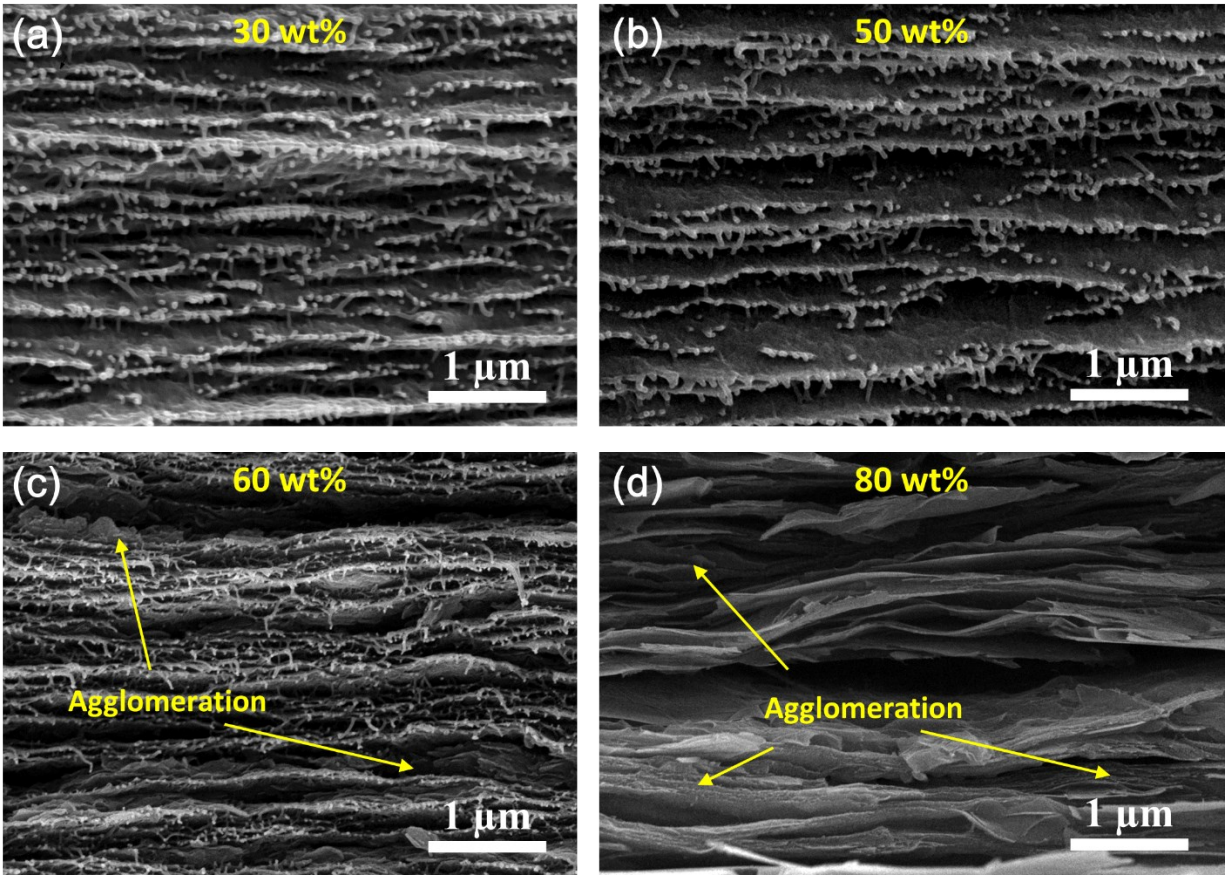

Figure S6. Cross-section SEM images of fGnP@PANF at different contents of fGnP (a) 30 wt%, (b) 50 wt%, (c) 60 wt%, and (d) 80 wt%.

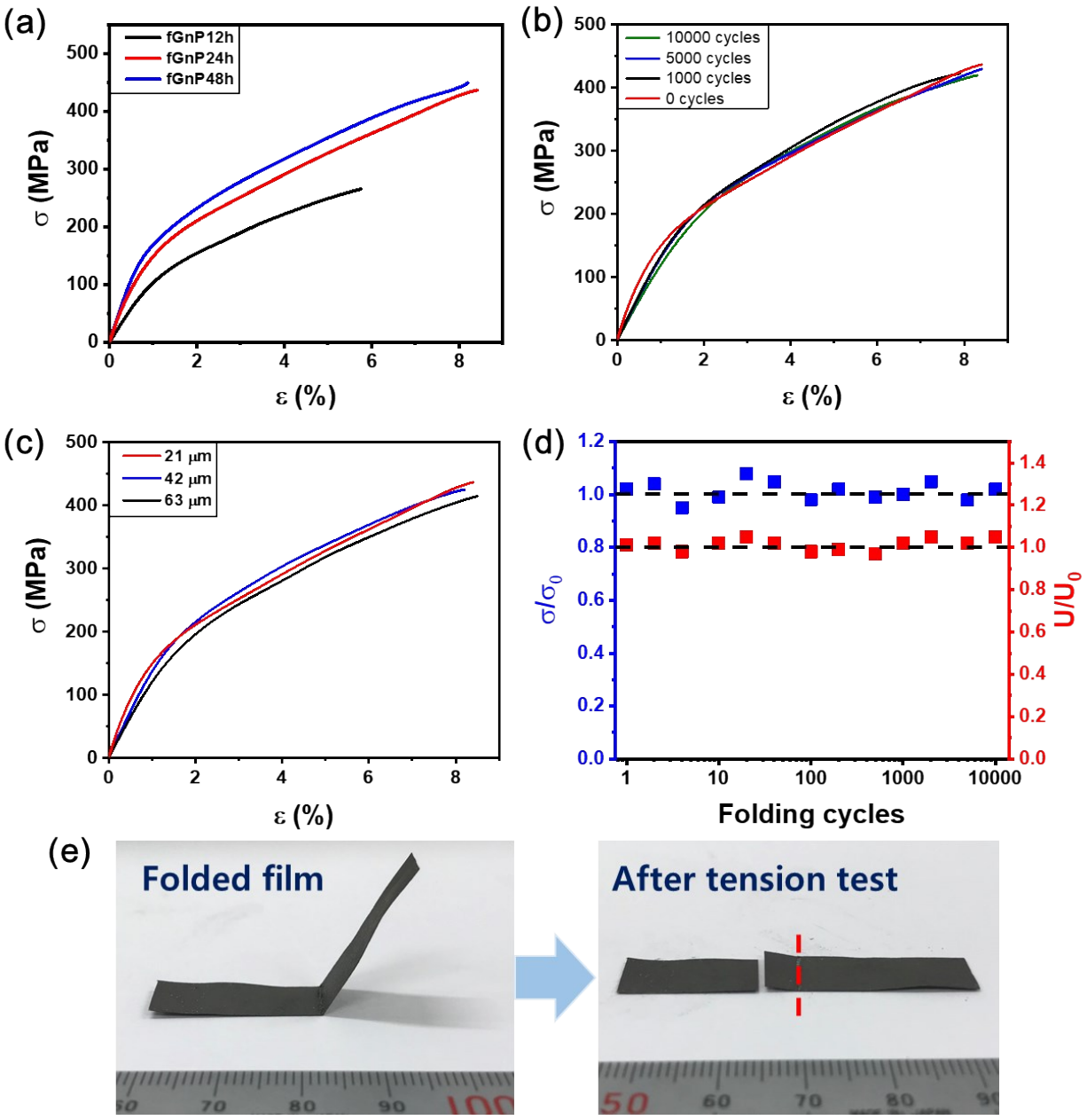

Figure S7. (a) Stress-strain curves of fGnP50@PANF papers undergone different folding cycles, (b) Stress-strain curves of fGnP50@PANF at different film thicknesses, (c) Relative tensile strength of fGnP50@PANF film undergone different folding cycles, (d) Relative toughness of fGnP50@PANF film undergone different folding cycles, (e) digital photo of folded fGnP50@PANF strip (left) and that after tensile test (right) showing that the fracture line different from the folding line (red dash line).

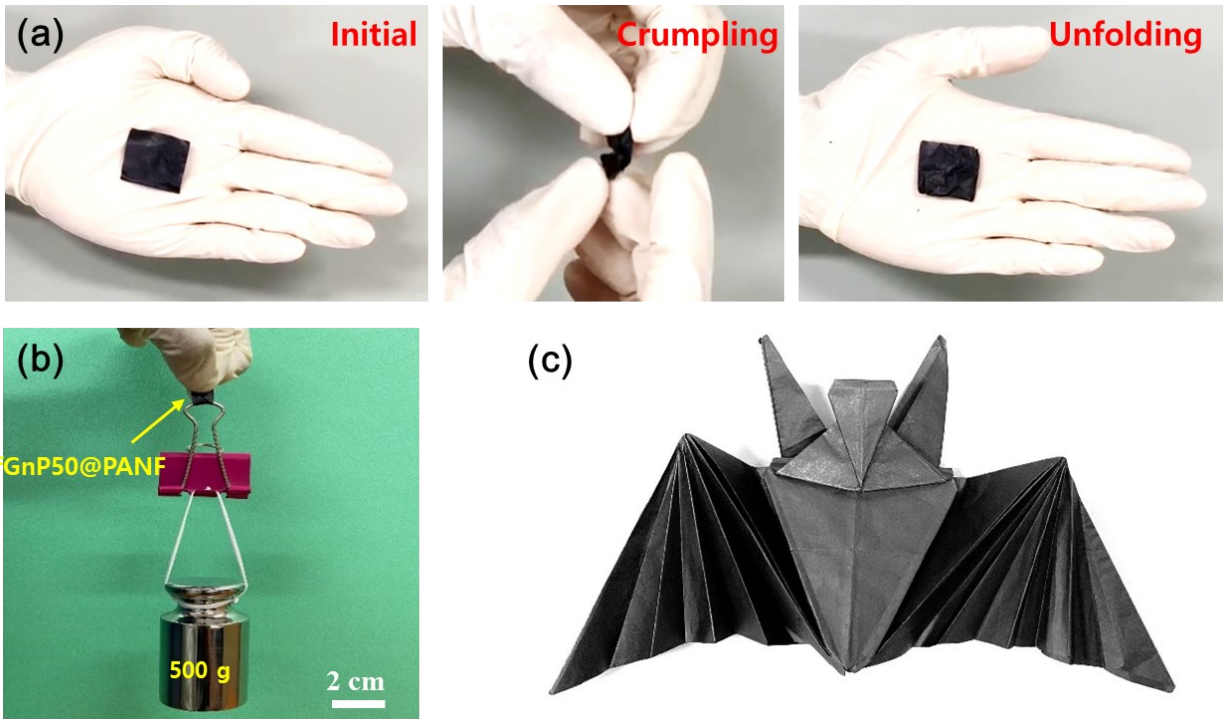

Figure S8. Digital photos of (a) the crumpling process of fGnP50@PANF film, (b) the crumpled fGnP50@PANF strip can withstand a weight of 500 g, and (c) the origami bat is shaped using fGnP50@PANF paper.

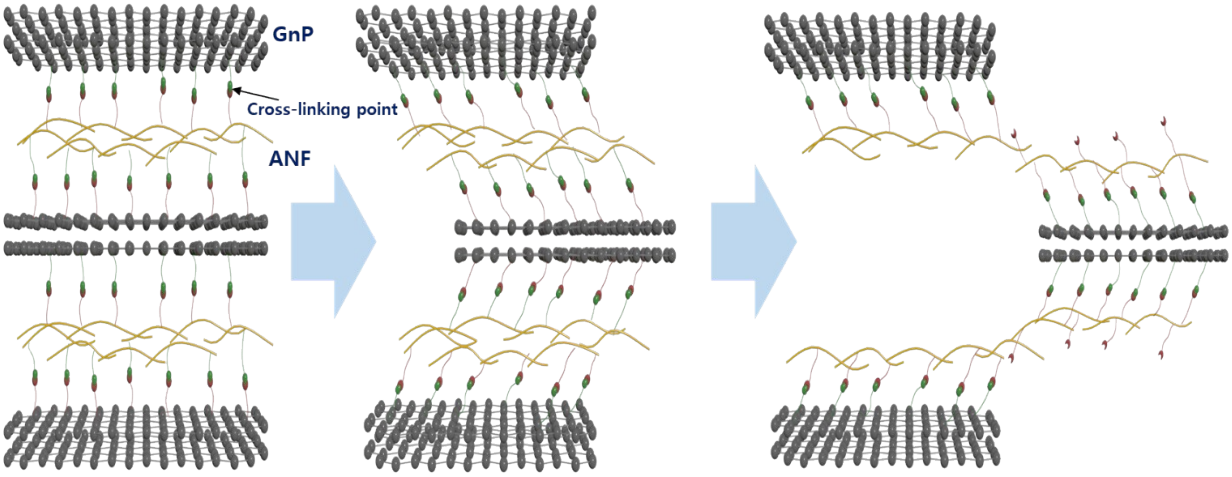

Figure S9. Schematic illustration of the fracture mechanism of the fGnP@PANF bioinspired paper.

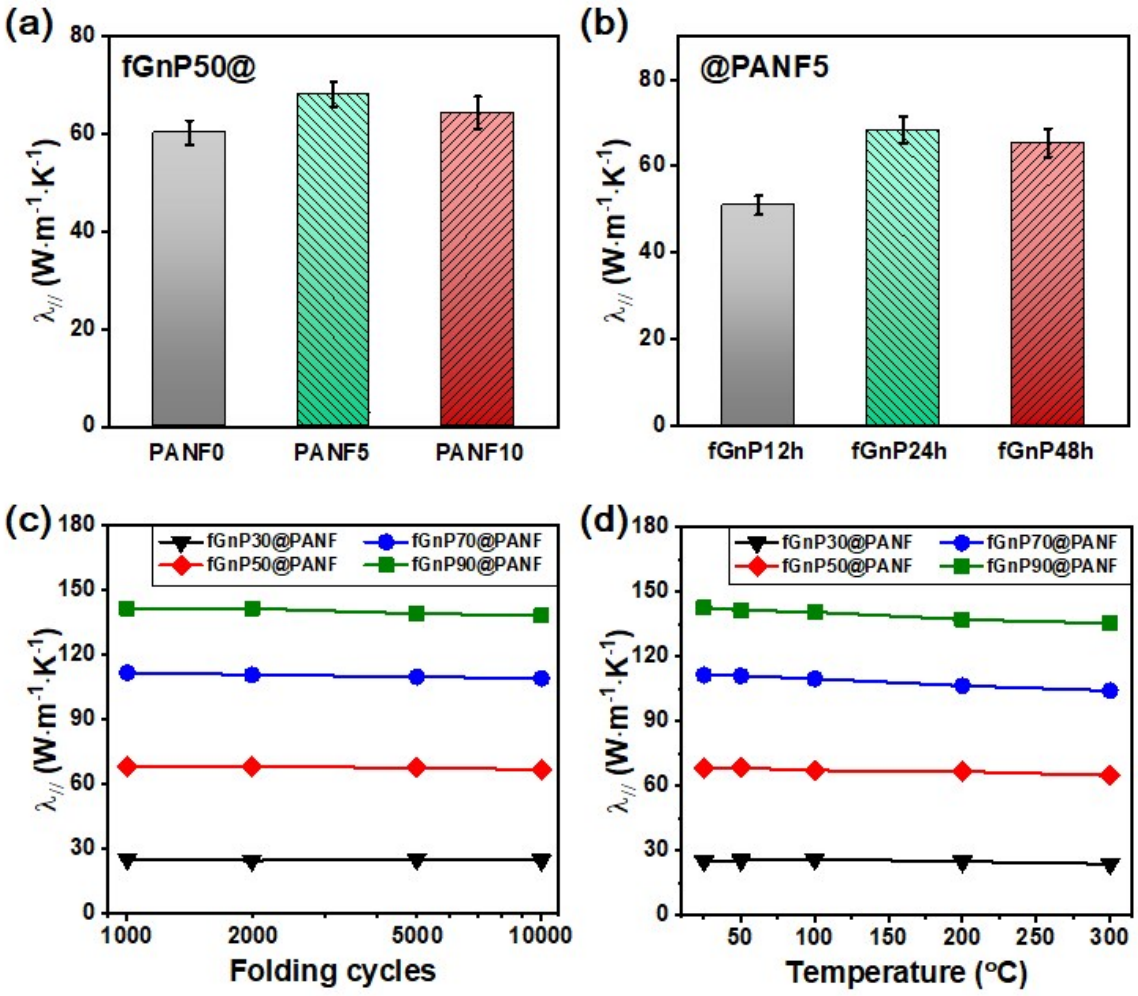

Figure S10. In-plane thermal conductivity of fGnP50@PANF bioinspired papers (a) using different contents of crosslinking agent, (b) using fGnP with different polymerization times (12 h, 24 h, and 48 h). In-plane thermal conductivity of fGnP50@PANF bioinspired papers at different contents of filler as a function of (c) folding cycle and (d) temperature.

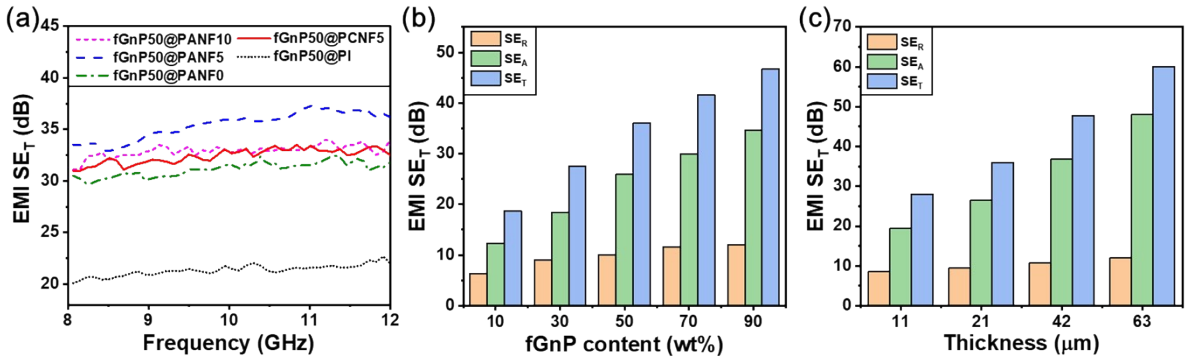

Figure S11. (a) EMI SE_T of the fGnP50@PANF bioinspired papers with different crosslinking agent and with the fGnP50@PCNF10 papers and the fGnP@PI films, (b) SE_R, SE_A and SE_T of fGnP@PANF bioinspired paper at different contents of filler at 10 GHz, and (c) SE_R, SE_A and SE_T of fGnP50@PANF bioinspired paper at different film thicknesses at 10 GHz.

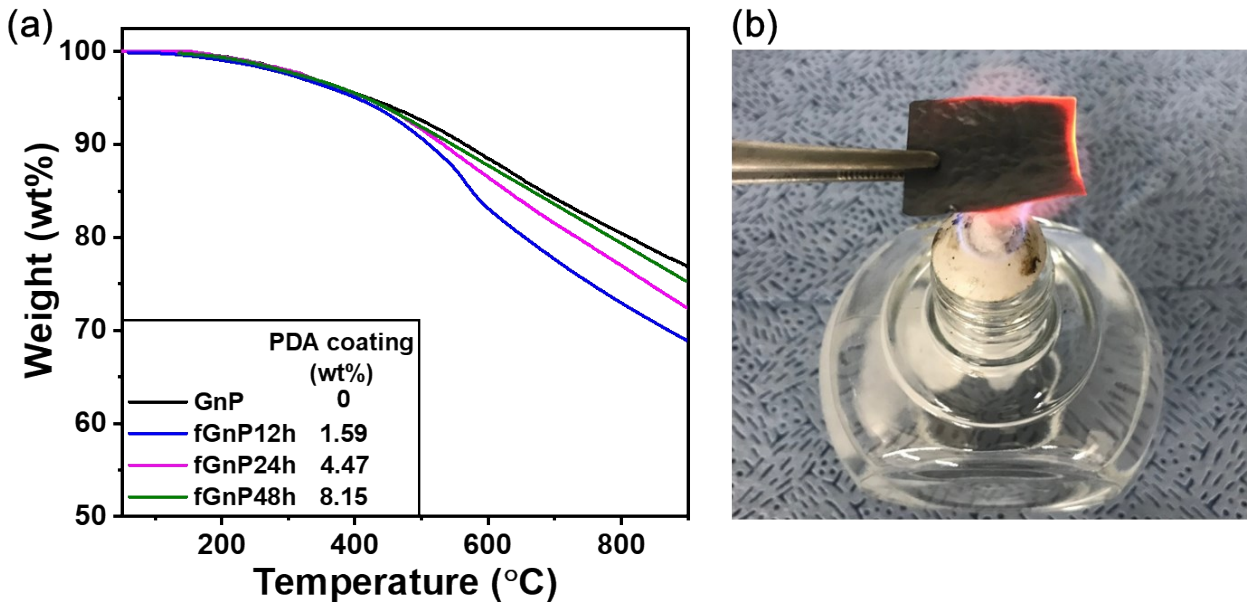

Figure S12. (a) TGA of fGnP treated PDA with different polymerization times (12 h, 24 h, and 48 h), and (b) the exposed fGnP50@PANF papers under alcohol flame after 5 h.

Table S1. A comparison on tensile strength and in-plane thermal conductivity of fGnP@PANF bioinspired papers with BN- and graphene-based 1D nanofibers films.

Materials	Loading (wt%)	σ_u (MPa)	$\lambda_{\parallel}$ ($W \cdot m^{-1} \cdot K^{-1}$)	Ref.
fGnP@PANF	30	309.1	25.2	**This work**
	50	437.3	68.2	
	60	266.2	85.3	
GS/CNF	50	72.3	164.7	Chen *et al.*[S1]
rGO/CNF	50	67.0	7.3	Yang *et al.* [S2]
GS/CNF	10	86.2	6.8	Song *et al.* [S3]
GPs/CNF	6	53.0	9.0	Song *et al.* [S4]
rGO/CNF	30	90.0	6.2	Song *et al.* [S5]
GnP/CNF	75	46.4	59.5	Li *et al.* [S6]
GnP/CNF	75	50.7	58.0	Wang *et al.* [S7]
GNS/PBONF	40	137.5	87.2	Wang *et al.* [S8]
	50	194.7	98.7	
	60	188.9	123.4	
BNNS/ANF	20	180	30.0	Wu *et al.* [S9]
	30	160.0	46.7	
	45	82	42.0	
BNNS/ANF	50	36.8	3.9	Ma *et al.* [S10]
BNNS/CNF	50	50.0	145.7	Zhu *et al.* [S11]
BNNS/CNF	70	60.0	30.3	Wu *et al.* [S12]
BNNS/CNF	60	45.5	24.3	Wu *et al.* [S13]
BNNS/CNF	25	45.0	22.7	Hu *et al.* [S14]

*CNF: cellulose nanofiber, GS: graphene sheets, rGO: reduced graphene oxide, PBONF: polybenzoxazone nanofiber, ANF: aramid nanofiber, BNNS: boron nitride nanosheets.

Table S2. A comparison on specific thermal conductivity between fGnP@ANF bioinspired papers with metal/alloy materials.

Materials	ρ ($g \cdot cm^{-3}$)	σ_u (MPa)	$\lambda_{\parallel}$ ($W \cdot m^{-1} \cdot K^{-1}$)	$\lambda_{\parallel}/\rho$ ($W \cdot m^{-1} \cdot K^{-1}/g \cdot cm^{-3}$)	σ/ρ ($MPa/g \cdot cm^{-3}$)
fGnP50@PANF	1.55	437	68.2	44.00	281.94
Stainless Steel (UNS S30400)	8.06	~620	~17	2.11	76.92
Fe	7.87	~540	~76.2	9.68	68.61
Aluminum Alloy (UNS A95182)	2.65	~275	~123	46.42	103.77
Copper Alloy (UNS C94500)	9.4	~170	~52	5.53	18.09
Ag	10.47	~340	~420	40.11	32.47
Au	19.3	~220	~300	15.54	11.40

*The properties of metal/alloy are taken from AZO Materials (www.azom.com).

Table S3. A comparison on the in-plane thermal conductivity enhancement per unit percent filler content between fGnP@PANF bioinspired papers with BN- and graphene-based 1D nanofibers films.

Filler	Matrix	Loading (wt%)	$\lambda_{\parallel}$ ($W \cdot m^{-1} \cdot K^{-1}$)	$\lambda_{\parallel}$/wt% ($W \cdot m^{-1} \cdot K^{-1}$/wt%)	Ref.
GnP	ANF	50	68.2	1.36	**This work**
GNS	PI	50	65.0	1.30	Wei *et al.*[S15]
rGO	CNF	50	7.3	0.15	Yang *et al.*[S2]
GS	CNF	10	6.8	0.68	Song *et al.*[S3]
frGO	CNF	6	9.0	1.50	Song *et al.*[S4]
rGO	CNF	30	6.2	0.21	Song *et al.*[S5]
GnP	CNF	75	59.5	0.79	Li *et al.*[S6]
GnP	CNF	75	58.0	0.77	Wang *et al.*[S7]
rGO	NR	50	20.84	0.42	Feng *et al.*[S16]
GF	PVA	93	61.3	0.66	Wang *et al.*[S17]
MLG	Epoxy	12	33.5	2.84	Li *et al.*[S18]
GP	Epoxy	20	5.0	0.25	Debelak *et al.*[S19]
MLG	Epoxy	20	5.2	0.26	Shahil *et al.*[S20]
BNNS	ANF	20	30.0	1.50	Wu *et al.*[S9]
		30	46.7	1.56	
		45	42.0	0.93	
BNNS	ANF	50	3.9	0.08	Ma *et al.*[S10]
BNNS	CNF	70	30.3	0.43	Wu *et al.*[S12]
BNNS	CNF	60	24.3	0.40	Wu *et al.*[S13]
BNNS	CNF	25	22.7	0.91	Hu *et al.*[S14]
BNNS	HDPE	40	3.57	0.09	Zhang *et al.*[S21]
BNNS	CNF	50	15.13	0.30	Hu *et al.*[S22]
BNNS	ANF	50	0.62	0.01	Lin *et al.*[S23]
BNNS	PI	12.4	4.25	0.34	Cao *et al.*[S24]
BNNT	CNF	25	21.39	0.86	Zeng *et al.*[S25]
BN	PU	95	50.3	0.53	Yu *et al.*[S26]
BNNS	PDMS	33	16.3	0.49	Chen *et al.*[S27]

*PBONF: polybenzoxazone nanofiber, GNS: graphene nanosheets, frGO: functionalized reduced graphene oxide, GF, graphene fluoride, NR: natural rubber, PVA: poly vinyl alcohol, MLG: mutil-layered graphene, GP: graphite, BNNS: boron nitride nanosheets, BNNT: boron nitride nanotubes, HDPE: High-density polyethylene, PI: polyimide, PU: polyurethane, PDMS: polydimethylsiloxane, CNF: cellulose nanofiber, ANF: aramid nanofiber.

Table S4. Coefficient of Reflection (R), Absorption (A) and Transmission (T) of fGnP@PANF bioinspired papers as a function of filler contents at 10 GHz.

fGnP contents (wt%)	R (%)	T (%)	A (%)
10	76.93	1.36	21.7
30	87.64	1.78×10^{-1}	12.18
50	88.89	2.50×10^{-2}	11.08
70	93.06	7.00×10^{-3}	6.93
90	93.72	2.15×10^{-3}	6.28

Table S5. Coefficient of Reflection (*R*), Absorption (*A*) and Transmission (*T*) of fGnP50@PANF bioinspired papers at different thicknesses at 10 GHz.

Thickness (μm)	*R* (%)	*T* (%)	*A* (%)
11	86.15	1.59×10^{-1}	13.69
21	88.89	2.50×10^{-2}	11.08
42	91.75	1.71×10^{-3}	8.25
63	93.72	9.9×10^{-5}	6.28

Table S6. A comparison on absolute effectiveness EMI SE between fGnP@PANF bioinspired papers with graphene, CNT and metal based polymer composites.

Materials	Loading (wt%)	t (mm)	ρ ($g \cdot cm^{-3}$)	$\lambda_{\parallel}$ ($W \cdot m^{-1} \cdot K^{-1}$)	SE_T (dB)	$ASSE_T$ ($dB \cdot cm^2 \cdot g^{-1}$)	Ref.
GnP/PS	35	3	1.43	4.72	33	77	Gou *et al.*[S28]
GnP/EP	50	1	1.55	8	45	290	Kargar *et al.*[S29]
GnP/PEDOT-PSS	25	0.8	1.35	0.83	70	648	Nidhi *et al.*[S30]
GnP@rGO/EP	21	3	1.32	1.56	51	129	Liang *et al.*[S31]
GS-Ni/PVDF	20	0.7	1.34	8.96	51.4	548	Liang *et al.*[S32]
GS-Fe-Ni/CE	20	3.5	1.32	4.13	55	119	Ren *et al.*[S33]
rGO/CNF	50	0.023	1.78	7.3	26.2	6400	Yang *et al.*[S2]
rGO@Fe_3O_4/EP	9	1	1.25	1.2	13.45	108	Liu *et al.*[S34]
rGO/WPU	3	1	1.22	2.13	45.6	374	Wang *et al.*[S35]
rGO/PEI	10	0.29	2.3	0.037	44	660	Shen *et al.*[S36]
rGO-Fe_3O_4/PEI	10	0.4	2.5	0.071	41.5	415	Shen *et al.*[S36]
CNT/EVA	70	0.065	1.65	17.9	32.4	3021	Wang *et al.*[S37]
CNT-Fe_3O_4/PVDF	8	1.1	1.25	0.62	35.6	259	Chen *et al.*[S38]
CNT-Fe_3O_4-Ag/EP	15	2	1.29	0.46	35	136	Wang *et al.*[S39]
CNT/PVDF	6	0.3	1.23	1.39	35.3	957	Li *et al.*[S40]
CuNWs/EP	7	3	1.28	0.51	47	122	Yang *et al.*[S41]
Cu/PCL	45	1	0.59	7	110.7	1876	Lee *et al.*[S42]
fGnP30@PANF	30	0.021	1.45	142.8	30.1	9031	**This work**
fGnP50@PANF	50	0.021	1.55	68.2	36.2	11060	
fGnP70@PANF	70	0.021	1.75	142.8	41.8	11319	
fGnP90@PANF	90	0.021	1.82	142.8	48.2	12218	

*PS: polystyrene, EP: epoxy, PEDOT-PSS: Poly(3,4-ethylenedioxythiophene)-poly(styrenesulfonate), PVDF: polyvinylidene difluoride, CE: cyanate ester, GS: graphene sheet, rGO: reduced graphene oxide, CNF: cellulose nanofiber, WPU: water-based polyurethane, PEI: polyetherimide, EVA: ethylene vinyl acetate, CNT: carbon nanotubes, CuNWs: copper nanowires, PCL: polycaprolactone.

References

(S1) Chen, Y.; Hou, X.; Kang, R.; Liang, Y.; Guo, L.; Dai, W.; Nishimura, K.; Lin, C. Te; Jiang, N.; Yu, J. Highly Flexible Biodegradable Cellulose Nanofiber/Graphene Heat-Spreader Films with Improved Mechanical Properties and Enhanced Thermal Conductivity. *J. Mater. Chem. C* **2018**, *6* (46), 12739–12745.

(S2) Yang, W.; Zhao, Z.; Wu, K.; Huang, R.; Liu, T.; Jiang, H.; Chen, F.; Fu, Q. Ultrathin Flexible Reduced Graphene Oxide/Cellulose Nanofiber Composite Films with Strongly Anisotropic Thermal Conductivity and Efficient Electromagnetic Interference Shielding. *J. Mater. Chem. C* **2017**, *5* (15), 3748–3756.

(S3) Song, N.; Cui, S.; Jiao, D.; Hou, X.; Ding, P.; Shi, L. Layered Nanofibrillated Cellulose Hybrid Films as Flexible Lateral Heat Spreaders: The Effect of Graphene Defect. *Carbon* **2017**, *115*, 338–346.

(S4) Song, N.; Hou, X.; Chen, L.; Cui, S.; Shi, L.; Ding, P. A Green Plastic Constructed from Cellulose and Functionalized Graphene with High Thermal Conductivity. *ACS Appl. Mater. Interfaces* **2017**, *9* (21), 17914–17922.

(S5) Song, N.; Jiao, D.; Ding, P.; Cui, S.; Tang, S.; Shi, L. Anisotropic Thermally Conductive Flexible Films Based on Nanofibrillated Cellulose and Aligned Graphene Nanosheets. *J. Mater. Chem. C* **2016**, *4* (2), 305–314.

(S6) Li, G.; Tian, X.; Xu, X.; Zhou, C.; Wu, J.; Li, Q.; Zhang, L.; Yang, F.; Li, Y. Fabrication of Robust and Highly Thermally Conductive Nanofibrillated Cellulose/Graphite Nanoplatelets Composite Papers. *Compos. Sci. Technol.* **2017**, *138*, 179–185.

(S7) Wang, F.; Drzal, L. T.; Qin, Y.; Huang, Z. Multifunctional Graphene Nanoplatelets/Cellulose Nanocrystals Composite Paper. *Compos. Part B Eng.* **2015**, *79*, 521–529.

(S8) Wang, Y.; Xia, S.; Li, H.; Wang, J. Unprecedentedly Tough, Folding-Endurance, and Multifunctional Graphene-Based Artificial Nacre with Predesigned 3D Nanofiber Network as Matrix. *Adv. Funct. Mater.* **2019**, *29* (38), 1903876.

(S9) Wu, K.; Wang, J.; Liu, D.; Lei, C.; Liu, D.; Lei, W.; Fu, Q. Highly Thermoconductive, Thermostable, and Super-Flexible Film by Engineering 1D Rigid Rod-Like Aramid Nanofiber/2D Boron Nitride Nanosheets. *Adv. Mater.* **2020**, *32* (8), 1906939.

(S10) Ma, T.; Zhao, Y.; Ruan, K.; Liu, X.; Zhang, J.; Guo, Y.; Yang, X.; Kong, J.; Gu, J. Highly Thermal Conductivities, Excellent Mechanical Robustness and Flexibility, and Outstanding Thermal Stabilities of Aramid Nanofiber Composite Papers with Nacre-Mimetic Layered Structures. *ACS Appl. Mater. Interfaces* **2020**, *12* (1), 1677–1686.

(S11) Zhu, H.; Li, Y.; Fang, Z.; Xu, J.; Cao, F.; Wan, J.; Preston, C.; Yang, B.; Hu, L. Highly Thermally Conductive Papers with Percolative Layered BNNS. *ACS Nano* **2014**, *8* (4), 3606–3613.

(S12) Wu, K.; Fang, J.; Ma, J.; Huang, R.; Chai, S.; Chen, F.; Fu, Q. Achieving a Collapsible, Strong, and Highly Thermally Conductive Film Based on Oriented Functionalized Boron Nitride Nanosheets and Cellulose Nanofiber. *ACS Appl. Mater. Interfaces* **2017**, *9* (35), 30035–30045.

(S13) Wu, K.; Liao, P.; Du, R.; Zhang, Q.; Chen, F.; Fu, Q. Preparation of a Thermally Conductive Biodegradable Cellulose Nanofiber/Hydroxylated Boron Nitride Nanosheet Film: The Critical Role of Edge-Hydroxylation. *J. Mater. Chem. A* **2018**, *6* (25), 11863–11873.

(S14) Hu, Z.; Wang, S.; Chen, G.; zhang, Q.; Wu, K.; Shi, J.; Liang, L.; Lu, M. An Aqueous-Only, Green Route to Exfoliate Boron Nitride for Preparation of High Thermal Conductive Boron Nitride Nanosheet/Cellulose Nanofiber Flexible Film. *Compos. Sci. Technol.* **2018**, *168*, 287–295.

(S15) Wei, Q.; Pei, S.; Qian, X.; Liu, H.; Liu, Z.; Zhang, W.; Zhou, T.; Zhang, Z.; Zhang, X.; Cheng, H.; Ren, W. Superhigh Electromagnetic Interference Shielding of Ultrathin Aligned Pristine Graphene Nanosheets Film. *Adv. Mater.* **2020**, *32* (14), 1907411.

(S16) Feng, C. P.; Chen, L. B.; Tian, G. L.; Wan, S. S.; Bai, L.; Bao, R. Y.; Liu, Z. Y.; Yang, M. B.; Yang, W. Multifunctional Thermal Management Materials with Excellent Heat Dissipation and Generation Capability for Future Electronics. *ACS Appl. Mater. Interfaces* **2019**, *11* (20), 18739–18745.

(S17) Wang, X.; Wu, P. Highly Thermally Conductive Fluorinated Graphene Films with Superior Electrical Insulation and Mechanical Flexibility. *ACS Appl. Mater. Interfaces* **2019,** *11* (24), 21946–21954.
(S18) Li, Q.; Guo, Y.; Li, W.; Qiu, S.; Zhu, C.; Wei, X.; Chen, M.; Liu, C.; Liao, S.; Gong, Y.; Mishra, A. K.; Liu, L. Ultrahigh Thermal Conductivity of Assembled Aligned Multilayer Graphene/Epoxy Composite. *Chem. Mater.* **2014**, *26* (15), 4459–4465.
(S19) Debelak, B.; Lafdi, K. Use of Exfoliated Graphite Filler to Enhance Polymer Physical Properties. *Carbon* **2007**, *45* (9), 1727–1734.
(S20) Shahil, K. M. F.; Balandin, A. A. Graphene-Multilayer Graphene Nanocomposites as Highly Efficient Thermal Interface Materials. *Nano Lett.* **2012**, *12* (2), 861–867.
(S21) Zhang, X.; Zhang, J.; Xia, L.; Li, C.; Wang, J.; Xu, F.; Zhang, X.; Wu, H.; Guo, S. Simple and Consecutive Melt Extrusion Method to Fabricate Thermally Conductive Composites with Highly Oriented Boron Nitrides. *ACS Appl. Mater. Interfaces* **2017**, *9* (27), 22977–22984.
(S22) Hu, D.; Ma, W.; Zhang, Z.; Ding, Y.; Wu, L. Dual Bio-Inspired Design of Highly Thermally Conductive and Superhydrophobic Nanocellulose Composite Films. *ACS Appl. Mater. Interfaces* **2020**, *12*, 11115–11125.
(S23) Lin, M.; Li, Y.; Xu, K.; Ou, Y.; Su, L.; Feng, X.; Li, J.; Qi, H.; Liu, D. Thermally Conductive Nanostructured, Aramid Dielectric Composite Films with Boron Nitride Nanosheets. *Compos. Sci. Technol.* **2019**, *175*, 85–91.
(S24) Cao, L.; Wang, J.; Dong, J.; Zhao, X.; Li, H. B.; Zhang, Q. Preparation of Highly Thermally Conductive and Electrically Insulating PI/BNNSs Nanocomposites by Hot-Pressing Self-Assembled PI/BNNSs Microspheres. *Compos. Part B Eng.* **2020**, *188*, 107882.
(S25) Zeng, X.; Sun, J.; Yao, Y.; Sun, R.; Xu, J. Bin; Wong, C. P. A Combination of Boron Nitride Nanotubes and Cellulose Nanofibers for the Preparation of a Nanocomposite with High Thermal Conductivity. *ACS Nano* **2017**, *11* (5), 5167–5178.
(S26) Yu, C.; Gong, W.; Tian, W.; Zhang, Q.; Xu, Y.; Lin, Z.; Hu, M.; Fan, X.; Yao, Y. Hot-Pressing Induced Alignment of Boron Nitride in Polyurethane for Composite Films with Thermal Conductivity over 50 $Wm^{-1} K^{-1}$. *Compos. Sci. Technol.* **2018**, *160*, 199–207.
(S27) Chen, J.; Huang, X.; Sun, B.; Jiang, P. Highly Thermally Conductive Yet Electrically Insulating Polymer/Boron Nitride Nanosheets Nanocomposite Films for Improved Thermal Management Capability. *ACS Nano* **2019**, *13* (1), 337–345.
(S28) Guo, Y.; Pan, L.; Yang, X.; Ruan, K.; Han, Y.; Kong, J.; Gu, J. Simultaneous Improvement of Thermal Conductivities and Electromagnetic Interference Shielding Performances in Polystyrene Composites via Constructing Interconnection Oriented Networks Based on Electrospinning Technology. *Compos. Part A Appl. Sci. Manuf.* **2019**, *124*, 105484.
(S29) Kargar, F.; Barani, Z.; Balinskiy, M.; Magana, A. S.; Lewis, J. S.; Balandin, A. A. Dual-Functional Graphene Composites for Electromagnetic Shielding and Thermal Management. *Adv. Electron. Mater.* **2019**, *5* (1), 1800558.
(S30) Agnihotri, N.; Chakrabarti, K.; De, A. Highly Efficient Electromagnetic Interference Shielding Using Graphite Nanoplatelet/Poly(3,4-Ethylenedioxythiophene)-Poly(Styrenesulfonate) Composites with Enhanced Thermal Conductivity. *RSC Adv.* **2015**, *5* (54), 43765–43771.
(S31) Liang, C.; Qiu, H.; Han, Y.; Gu, H.; Song, P.; Wang, L.; Kong, J.; Cao, D.; Gu, J. Superior Electromagnetic Interference Shielding 3D Graphene Nanoplatelets/Reduced Graphene Oxide Foam/Epoxy Nanocomposites with High Thermal Conductivity. *J. Mater. Chem. C* **2019**, *7* (9), 2725–2733.
(S32) Liang, L.; Xu, P.; Wang, Y.; Shang, Y.; Ma, J.; Su, F.; Feng, Y.; He, C.; Wang, Y.; Liu, C. Flexible Polyvinylidene Fluoride Film with Alternating Oriented Graphene/Ni Nanochains for Electromagnetic Interference Shielding and Thermal Management. *Chem. Eng. J.* **2020**, *395*, 125209.
(S33) Ren, F.; Song, D.; Li, Z.; Jia, L.; Zhao, Y.; Yan, D.; Ren, P. Synergistic Effect of Graphene Nanosheets and Carbonyl Iron-Nickel Alloy Hybrid Filler on Electromagnetic Interference Shielding and Thermal Conductivity of Cyanate Ester Composites. *J. Mater. Chem. C* **2018**, *6* (6), 1476–1486.

(S34) Liu, Y.; Lu, M.; Wu, K.; Yao, S.; Du, X.; Chen, G.; Zhang, Q.; Liang, L.; Lu, M. Anisotropic Thermal Conductivity and Electromagnetic Interference Shielding of Epoxy Nanocomposites Based on Magnetic Driving Reduced Graphene Oxide@Fe3O4. *Compos. Sci. Technol.* **2019**, *174*, 1–10.
(S35) Wang, Y.; Wang, W.; Xu, R.; Zhu, M.; Yu, D. Flexible, Durable and Thermal Conducting Thiol-Modified RGO-WPU/Cotton Fabric for Robust Electromagnetic Interference Shielding. *Chem. Eng. J.* **2019**, *360*, 817–828.
(S36) Shen, B.; Zhai, W.; Tao, M.; Ling, J.; Zheng, W. Lightweight, Multifunctional Polyetherimide/Graphene@Fe3O 4 Composite Foams for Shielding of Electromagnetic Pollution. *ACS Appl. Mater. Interfaces* **2013**, *5* (21), 11383–11391.
(S37) Wang, Z. G.; Yang, Y. L.; Zheng, Z. L.; Lan, R. T.; Dai, K.; Xu, L.; Huang, H. D.; Tang, J. H.; Xu, J. Z.; Li, Z. M. Achieving Excellent Thermally Conductive and Electromagnetic Shielding Performance by Nondestructive Functionalization and Oriented Arrangement of Carbon Nanotubes in Composite Films. *Compos. Sci. Technol.* **2020**, *194*, 108190.
(S38) Cheng, H.; Wei, S.; Ji, Y.; Zhai, J.; Zhang, X.; Chen, J.; Shen, C. Synergetic Effect of Fe 3 O 4 Nanoparticles and Carbon on Flexible Poly (Vinylidence Fluoride) Based Films with Higher Heat Dissipation to Improve Electromagnetic Shielding. *Compos. Part A Appl. Sci. Manuf.* **2019**, *121*, 139–148.
(S39) Wang, L.; Qiu, H.; Liang, C.; Song, P.; Han, Y.; Han, Y.; Gu, J.; Kong, J.; Pan, D.; Guo, Z. Electromagnetic Interference Shielding MWCNT-Fe3O4@Ag/Epoxy Nanocomposites with Satisfactory Thermal Conductivity and High Thermal Stability. *Carbon* **2019**, *141*, 506–514.
(S40) Li, X.; Zeng, S.; Shiju, E.; Liang, L.; Bai, Z.; Zhou, Y.; Zhao, B.; Zhang, R. Quick Heat Dissipation in Absorption-Dominated Microwave Shielding Properties of Flexible Poly(Vinylidene Fluoride)/Carbon Nanotube/Co Composite Films with Anisotropy-Shaped Co (Flowers or Chains). *ACS Appl. Mater. Interfaces* **2018**, *10* (47), 40789–40799.
(S41) Yang, X.; Fan, S.; Li, Y.; Guo, Y.; Li, Y.; Ruan, K.; Zhang, S.; Zhang, J.; Kong, J.; Gu, J. Synchronously Improved Electromagnetic Interference Shielding and Thermal Conductivity for Epoxy Nanocomposites by Constructing 3D Copper Nanowires/Thermally Annealed Graphene Aerogel Framework. *Compos. Part A Appl. Sci. Manuf.* **2020**, *128*, 105670.
(S42) Lee, S. H.; Yu, S.; Shahzad, F.; Kim, W. N.; Park, C.; Hong, S. M.; Koo, C. M. Density-Tunable Lightweight Polymer Composites with Dual-Functional Ability of Efficient EMI Shielding and Heat Dissipation. *Nanoscale* **2017**, *9* (36), 13432–13440.